Atmospheric Research 305 (2024) 107444

Contents lists available at ScienceDirect

Atmospheric Research

journal homepage: www.elsevier.com/locate/atmosres

Sensitivity of surface downward longwave radiation to aerosol optical depth over the Lake Taihu region, China

Cheng Liu [a], Jianping Huang [b,*], Cheng Hu [c], Chang Cao [d], Kun Yue [e], Xiaozhen Fang [a], Renguo Zhu [a], Xuhui Lee [f]

[a] Jiangxi Provincial Key Laboratory of Genesis and Remediation of Groundwater Pollution/School of Water Resources and Environmental Engineering, East China University of Technology, Nanchang 330013, China
[b] Environmental Modeling Center, NOAA National Centers for Environmental Prediction, College Park, MD, USA
[c] College of Ecology and the Environment, Joint Center for sustainable Forestry in Southern China, Nanjing Forestry University, Nanjing 210037, China
[d] Center on Atmospheric Environment, International Joint Laboratory on Climate and Environment Change (ILCEC), Nanjing University of Information Science & Technology, Nanjing 210044, China
[e] Ecological and Agricultural Meteorological Center of Inner Mongolia, Huhhot 010051, China
[f] School of the Environment, Yale University, New Haven, CT 06511, USA

ARTICLE INFO

Keywords:
Downward longwave radiation
Aerosol optical depth
Lake Taihu
MERRA-2
Radiative transfer model

ABSTRACT

Downward longwave radiation (DLR) is an important component of the global radiation budget, significantly influencing surface energy dynamics. Accurate quantification of aerosol impacts on surface DLR is crucial for refining numerical weather predictions and comprehending surface energy balance. While the impact of aerosols on downward shortwave radiation has garnered substantial attention, investigation into the longwave radiation effect of aerosols remains relatively limited. In this study, the impact of aerosols on surface DLR is quantified by using continuous radiation data, conventional meteorological observations, and aerosol optical depth (AOD) retrieved from the Moderate Resolution Imaging Spectroradiometer (MODIS) satellite. These datasets span the period from 2011 to 2018 and are obtained from six stations of the Lake Taihu Flux Observational Network situated in Eastern China. The sensitivity of DLR to AOD (dDLR/dAOD) is determined through multiple linear regressions using both observational data and the Modern-Era Retrospective analysis for Research and Applications, Version 2 (MERRA-2) reanalysis. Additionally, a radiative transfer model is employed to derive the dDLR/dAOD. A three-variable linear regression of the observational data shows that DLR increases by 4.66 ± 1.99 W m^{-2} per unit increase in AOD (mean ± 1 standard deviation) under clear-sky conditions. The radiative transfer model and the three-variable linear regression of MERRA-2 reanalysis yield similar sensitivity values of 4.69 ± 1.23 W m^{-2} AOD^{-1} and 4.10 ± 0.25 W m^{-2} AOD^{-1}, respectively. However, these sensitivity values are considerably smaller than those reported in previous studies. Plausible factors contributing to the observed variance in sensitivity values are discussed. These results help to improve our understanding on the aerosol longwave radiation effect over the Lake Taihu region in Eastern China.

1. Introduction

Downward atmospheric longwave radiation (DLR), one of the largest terms in the surface energy balance, plays a crucial role in global radiation balance and climate change research (Wacker et al., 2011; Wang and Liang, 2009; Viúdez-Mora et al., 2009). Compared to the downward shortwave radiation, direct observations of DLR remain scarce. A precise understanding of DLR and its driving factors is essential for various applications, including land-surface exchange (Wang et al., 2017), climate change (Viúdez-Mora et al., 2009), and weather model predictions (Cho et al., 2008; Maghrabi et al., 2019; García et al., 2018).

Under clear-sky conditions, water vapor and air temperature at screen level are the two most important factors in determining DLR. As a result, most physical parameterizations of the clear-sky DLR are developed primarily based on these two factors (e.g., Brunt, 1932; Brutsaert, 1975; Idso, 1981; Prata, 1996). Even though generally omitted by these DLR parameterizations, aerosols are known to scatter and absorb terrestrial radiation (Panicker et al., 2008; Liu et al., 2019) and emit

* Corresponding author.
E-mail address: hjpfwj@gmail.com (J. Huang).

https://doi.org/10.1016/j.atmosres.2024.107444
Received 15 January 2024; Received in revised form 6 April 2024; Accepted 24 April 2024
Available online 26 April 2024

radiation energy in the longwave (Dufresne et al., 2002). The aerosol surface longwave radiation effect has received less attention than its shortwave radiation effect, and is usually ignored in climate models (Vogelmann et al., 2003; Hansell et al., 2010). In several observational studies, the aerosol-induced DLR effect is comparable to or greater than the radiative forcing of greenhouse gases, potentially offsetting a substantial proportion (10% to 51%) of shortwave radiation reduction under aerosol-polluted conditions (Vogelmann et al., 2003; Antón et al., 2014). Overlooking aerosol effect on DLR may lead to significant errors in climate models, especially in areas with pronounced aerosol pollution.

The efficiency of aerosol longwave radiative forcing is often quantified as the sensitivity of DLR to aerosol optical depth (AOD). This sensitivity, denoted as dDLR/dAOD (W m^{-2} AOD^{-1}), measures the amount of variation in DLR due to a unit change in AOD. The published studies on dDLR/dAOD have mainly focused on heavy pollution conditions and short time periods of approximately 1 day to 3 months, revealing a wide range of variability. For example, Markowicz et al. (2003) observed a dDLR/dAOD of 55 W m^{-2} AOD^{-1} for boundary-layer aerosols and 37 W m^{-2} AOD^{-1} for elevated dust aerosols during the Aerosol Characterization Experiment, ACE-Asia. At three ChinaFlux sites subject to industrial and desert dust pollution, dDLR/dAOD ranged from 24 to 62 W m^{-2} AOD^{-1} (Cao et al., 2016). Slightly lower sensitivity values (i.e., 20.8 and 24.8 W m^{-2} AOD^{-1}) were found based on two calculation methods for an urban site in Indian (Panicker et al., 2008), while a large sensitivity value of 46.3 W m^{-2} AOD^{-1} was obtained through linear regression between DLR and AOD observed in Saudi Arabia (Maghrabi et al., 2022). Notably, a strong Saharan dust event in southeastern Spain showed a 20 W m^{-2} increase in DLR for each AOD unit increment (Antón et al., 2014). Varied DLR sensitivities of 16 and 31 to 35 W m^{-2} AOD^{-1} were reported during the NASA African Monsoon Multidisciplinary Analysis (NAMMA) 2006 field campaign and the Asian Monsoon Years field experiment in China, respectively (Hansell et al., 2010, 2012). A radiative transfer modeling study showed sensitivities of 4.9 W m^{-2} AOD^{-1} and 6.2 W m^{-2} AOD^{-1} for rural and urban aerosols, respectively, which are significantly smaller than that for dust aerosols (i.e., 29.8 W m^{-2} AOD^{-1}; Wang et al., 2017). Overall, these studies demonstrate an important effect of aerosols on DLR, but the impact varies considerably with aerosol types and regions.

The Lake Taihu region is situated in the Yangtze River Delta, the most economically developed area in China, and has experienced heavy aerosol pollution due to rapid increase in anthropogenic emissions over the past decades (e.g., Shu et al., 2017; Huang et al., 2020). While aerosol shortwave radiative effects have been extensively studied in this region (e.g., Sun et al., 2017; Zhuang et al., 2018; Sun et al., 2019a; Yu et al., 2019; Liu et al., 2021), aerosol impact on DLR remains underexplored. In this study, long-term continuous radiation measurements and Moderate-resolution Imaging Spectroradiometer (MODIS) satellite-derived AOD product at six stations of the Lake Taihu Flux Observational Network from 2011 to 2018 are presented, together with Modern-Era Retrospective analysis for Research and Applications, Version 2 (MERRA-2) reanalysis dataset. Leveraging multiple variable linear regression and radiative transfer model, we aim to quantify the sensitivity of DLR to AOD (dDLR/dAOD) in the Lake Taihu region, and to determine whether the sensitivities estimated from radiative model and calculated with MERRA-2 reanalysis are consistent with those derived from observations.

2. Data and methods

2.1. Observational data in the Lake Taihu

The DLR was measured by the four-way net radiometers (model CNR4; Kipp & Zonen B.V., Delft, the Netherlands) at the six observational sites over the Lake Taihu (site ID: BFG, DPK, DS, MLW, PTS, and XLS; Fig. 1). The spectral range of CNR4 radiometer for longwave is

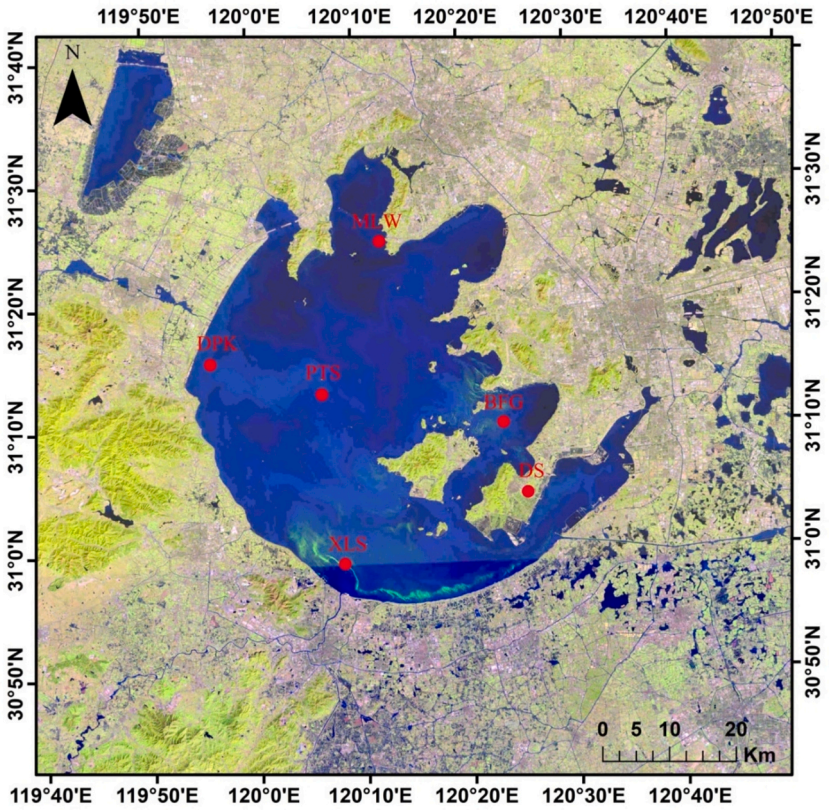

Fig. 1. A Landsat 9 natural color image of Lake Taihu (taken on 22 February 2022) and the location of six observational sites (red circles). (For interpretation of the references to color in this figure legend, the reader is referred to the web version of this article.)

4.5–42 μm. The dataset spans the period from January 2011 to December 2018 and has a half-hour temporal resolution. Concurrently, meteorological variables such as atmospheric pressure, relative humidity, and air temperature were measured at the same six sites. For information about the observational sites and the instruments, the reader is referred to the papers by Zhang et al. (2020) and Lee et al. (2014).

Due to the lack of direct ground-based observation in longwave AOD, visible AOD (i.e., 550 nm) is obtained from MODIS sensor on the Aqua and Terra satellites at a 3-km resolution (MOD04_3K for Terra and MYD04_3K for Aqua) (Levy et al., 2015). Note that we use visible AOD (550 nm) to establish the relationship with DLR in our study for the sake of convenience to compare the results with findings from previous studies (e.g., Panicker et al., 2008; Antón et al., 2014; Hansell et al., 2010, 2012; Cao et al., 2016; Maghrabi et al., 2022), though AOD decreases with increasing wavelength and is related to Ångström exponent for different types of aerosols. The Terra and Aqua satellites passed over the Lake Taihu region at around 10:30 and 13:30 local standard time, respectively. The radiation data collected during MODIS satellite overpasses were used to establish the relationship between DLR and AOD. The MODIS algorithm masks out any pixel that contains clouds (Remer et al., 2013). Thus, the dataset is suitable for quantifying aerosol radiative impact on DLR under cloudless daytime conditions. To ensure sufficient numbers of valid data points, a set of 3 × 3 pixels with high-quality AOD data (quality flag = 3) derived from dark target algorithms around the six observational sites was used for statistical analyses. These ground-based measurements of DLR, air temperature and relative humidity, together with satellite-observed AOD are utilized to determine the DLR sensitivity to AOD, following the procedure described in section 2.3.

2.2. MERRA-2 reanalysis data

MERRA-2 is an atmosphere reanalysis dataset developed by the NASA Global Modeling and Assimilation Office with a spatial resolution of 0.5° × 0.625° (latitude × longitude) (Gelaro et al., 2017). It can serve as a valuable data source when observational data is not readily available. By utilizing MERRA-2 data to calculate the sensitivity of DLR to AOD, we aim to investigate whether this commonly-used dataset can accurately estimate the sensitivity consistent with that derived from observations.

For a comparison, hourly AOD in 550 nm (data collection: tavg1_2d_aer_Nx), DLR under clear-sky and all-sky condition (tavg1_2d_rad_Nx), air temperature, and humidity (tavg1_2d_slv_Nx) from MERRA-2 were also utilized to determine the DLR sensitivity to AOD via multiple linear regressions described in section 2.3. Details about MERRA-2 data collection and variables used in this study are given in Table S1. Four-grid averages over the area of 31° N to 31.5° N in latitude and 120° E to 120.625° E in longitude were used to represent the Lake Taihu region. Although MERRA-2 assimilates several AOD datasets including bias-corrected AOD from MODIS (Cao et al., 2021), several studies found that MERRA-2 AOD is lower than the MODIS AOD and ground observations (Sun et al., 2019b; Gueymard and Yang, 2020; Che et al., 2022).

2.3. Determination of DLR sensitivity to AOD with multiple linear regressions

We first performed a linear regression analysis of the observational data. In this regression analysis, DLR is described as a three-parameter function:

$$DLR = a + bT_a + ce_a + dAOD \quad (1)$$

where T_a is air temperature, e_a is water vapor pressure (hPa); a represents intercept, and coefficients b, c and d represent DLR sensitivity to temperature (W m^{-2} K^{-1}), water vapor pressure (W m^{-2} hPa^{-1}), and AOD (W m^{-2} AOD^{-1}), respectively. In this function, the regression coefficient is estimated by using the least square method. There are a total of 676 data points used for the regression with either observations or MERRA-2 reanalysis.

The temperature and humidity sensitivities values were also determined with the DLR parameterization:

$$DLR = \varepsilon_a \sigma T_a^4 \quad (2)$$

where σ is the Stefan–Boltzmann constant, T_a is air temperature in K, and ε_a is apparent atmospheric emissivity. In this study, ε_a was computed from the Brutsaert (1975) clear-sky formula:

$$\varepsilon_a = 1.24(e_a/T_a)^{1/7} \quad (3)$$

The sensitivity of DLR to temperature ($\Delta DLR/\Delta T_a$) and water vapor pressure ($\Delta DLR/\Delta e_a$) were obtained by differentiation of Eq. (2) as:

$$\Delta DLR/\Delta T_a \approx 4.78\sigma T_a^{20/7} e_a^{1/7} \quad (4)$$

$$\Delta DLR/\Delta e_a \approx 0.177\sigma T_a^{27/7} e_a^{-6/7} \quad (5)$$

2.4. Calculations of DLR sensitivity to AOD with radiative transfer model

To further understand the DLR sensitivity to AOD, the Santa Barbara Discrete Ordinate Radiative Transfer Model (SBDART) model was employed to simulate the surface DLR over a range of aerosol-polluted conditions. The model has been widely adopted for the calculation of DLR and the associated aerosol radiative forcing (Ricchiazzi et al., 1998; Dufresne et al., 2002; Viúdez-Mora et al., 2009; Panicker et al., 2008). The model inputs include time, longitude and latitude, surface albedo, atmospheric vertical profile of temperature, humidity and ozone, and aerosol optical parameters such as AOD, single scattering albedo (SSA), and asymmetric factor (ASY). The surface type is specific as lake water, and the surface albedo is correspondingly determined with the model pre-defined values between 0.35 and 1.0 μm. The aerosol optical parameters were determined by the model-predefined boundary-layer aerosol types (e.g., rural, urban, oceanic) or defined by the user. Here, the monthly-averaged 550-nm SSA was retrieved from MERRA-2 reanalysis (Xu et al., 2022), while 550-nm ASY was acquired from the observations in the Lake Taihu region during 2006–2009 (Liu et al., 2012). Then the wavelength-dependent SSA and ASY were obtained by extrapolating 550-nm value to other wavelength based on the similar wavelength distribution pattern of rural aerosols. The obtained wavelength distribution of SSA and ASY in the Lake Taihu and their values for other aerosol types were compared in Fig. S3. Given that the lack of sounding in the Lake Taihu, we acquired monthly mean radio sounding observation from the Integrated Global Radiosonde Archive (Durre et al., 2016) for surrounding cities near the Lake Taihu, such as Shanghai (85 km away), Hangzhou (72 km away), and Nanjing (150 km away). A total of 288 radiosonde profiles from 2011 to 2018 were averaged across these three observational sites to represent the atmospheric conditions over the Lake Taihu region in the simulations. As shown in Fig. S1, the main differences in temperature and water vapor between radio sounding observations and SBDART model-default profiles were found below the 300-hPa level.

Several sensitivity experiments were completed with varying AODs, aerosol types and atmosphere conditions. For each simulation, the SBDART was run with 16 streams, which was considered an optimal stream number for achieving accurate flux calculations (Viúdez-Mora et al., 2009). The volume mixing ratios of CO_2, CH_4 and N_2O were set to 412 ppm, 1.875 ppm, and 0.33 ppm, respectively according to the year 2022 global background observations (https://gml.noaa.gov/ccgg/trends/, last access: September 26, 2022). The spectral DLR was calculated in the range of 4 to 40 μm at an interval of 1% in wavelength. The total DLR was obtained through integration of the spectral DLR over the range of 4 to 40 μm. The DLR forcing (DLRF) is defined as the DLR

difference under aerosol-polluted and aerosol-free conditions. The DLR sensitivity to AOD was derived through linear regression between the modeled DLRF and AOD (Panicker et al., 2008; Wang et al., 2017).

3. Results

3.1. Long-term variations of AOD, DLR and meteorological variables

The inter-annual variations of AOD, DLR, T_a and e_a at the DPK site from 2011 to 2018 are presented as an example in Fig. 2. The annual averages and trends for these variables in all the sites are detailed in Table 1. The annual mean of 550-nm AOD at the DPK site shows a decreasing trend over the period 2011 to 2018 with a regression slope of -0.046 yr^{-1} and a range of 0.75 to 1.21. A similar decreasing pattern was observed at the other sites, although the magnitude is slightly different (varying between -0.015 and -0.038 yr^{-1}). The decreasing trend suggests that the aerosol pollution was alleviated due to the implementation of strict emission reduction measures in China since 2013 (Zhang and Geng, 2019). A similar decreasing trend of AOD was also reported in other studies. For example, He et al. (2020) found a decreasing trend of -0.02 yr^{-1} in AOD during 2010 to 2016, while Filonchyk et al. (2019) reported a declining AOD trend of -0.04 yr^{-1} from 2008 to 2017 in the Yangtze River Basin of China.

The annual mean DLR at the DPK site varies in the range of 362.0 to 374.3 W m^{-2}, showing a significant increasing rate (1.46 W m^{-2} yr^{-1}, $p < 0.01$) during 2011 to 2018, which is comparable to that at other lake sites (i.e., 1.14 to 1.60 W m^{-2} yr^{-1}, $p < 0.05$). The DS site (a land site) shows a subtle decline trend (-0.89 W m^{-2} yr^{-1}, $p = 0.32$), probably due to significant data gaps as highlighted by Zhang et al. (2020). The DLR variation trends are consistent to those presented by Xiao et al. (2020), in which the DLR shows an increasing trend of 1.7 W m^{-2} yr^{-1} at BFG site from 2011 to 2017. The annual mean T_a and e_a, which are closely related to DLR, show clear increasing trends. The increasing rates for T_a and e_a are in ranges of 0.07 to 0.19 °C yr^{-1} and 0.07 to 0.50 hPa yr^{-1}, respectively, across the Lake Taihu area (as indicated in Table 1).

3.2. DLR sensitivity calculated with observational data

Fig. 3 depicts the dependence of DLR on T_a, e_a, and AOD. In these scatter plots, each data point represents one half-hourly observation at each of the six sites. A significant and positive correlation is observed between DLR and AOD (linear correlation coefficient $r = 0.25$, $p < 0.01$), although the coefficient is lower than that with T_a and e_a (0.96 and 0.94, respectively; $p < 0.01$). The relatively diminished correlation coefficient and increased variability between DLR and AOD (Fig. 3a) than that with T_a and e_a indicate that the T_a and e_a are the predominant factors controlling the variations in DLR though AOD exerts an important impact on DLR.

We further evaluate the relationship of DLR with the three variables by using multiple linear regressions for each site (Eq. 1). The regressions explain 95% to 99% of the observed variability (R^2) at the statistically high significance level $p < 0.001$. Table 2 presents the respective fitted coefficients for the three variables at each site. The sensitivity of DLR to T_a and e_a is in the range of 4.07 to 5.44 W m^{-2} K^{-1} and of 2.56 to 3.07 W m^{-2} hPa^{-1}, respectively, with the six-site mean of 4.24 ($\pm$ 0.21) W m^{-2} K^{-1} and 2.98 ($\pm$ 0.22) W m^{-2} hPa^{-1} (mean $\pm$ 1 standard deviation of spatial replicates). Meanwhile, the sensitivity of DLR to AOD fluctuates between 3.02 and 8.80 W m^{-2} AOD^{-1} with an average sensitivity of 4.66 ($\pm$1.99) W m^{-2} AOD^{-1} across the lake. The sensitivity values at DPK and DS are higher than other sites, probably due to smaller water vapor content in DS (a land site) and larger variability of meteorological conditions in these two sites (Table 1). The coefficients obtained from the three-variable regression are much smaller than the slope coefficients derived from the simple one-variable linear regression shown in Fig. 3, especially for AOD, implying that single-factor regression analysis exaggerates the effect of aerosols.

Table 3 shows the sensitivity of DLR to T_a and e_a derived from the DLR parameterization (Eqs. 4 and 5). The calculations show the sensitivity is in the range of 4.11 to 4.48 W m^{-2} K^{-1} for T_a and 3.0 to 3.80 W m^{-2} hPa^{-1} for e_a, with the means of 4.32 W m^{-2} K^{-1} and 3.33 W m^{-2} hPa^{-1} for the entire Lake Taihu. These results are consistent with those obtained through the multivariate linear regression (Table 2).

3.3. DLR sensitivity calculated using MERRA-2 reanalysis

Fig. 4 displays a comparison between MERRA-2 hourly data and the observations in the Lake Taihu. The MERRA-2 AOD is biased low in comparison with the MODIS AOD, with a regression slope of 0.38.

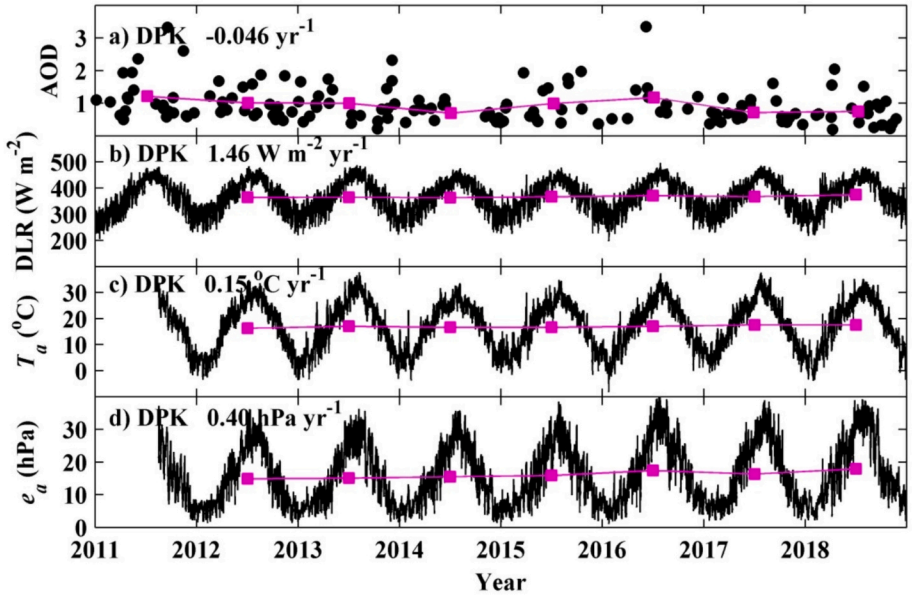

Fig. 2. Time series of hourly (black) and annual (magenta) means of a) MODIS-derived AOD, b) observed downward longwave radiation (DLR), c) observed air temperature (T_a), and e) observed water vapor pressure (e_a) at the DPK site. (For interpretation of the references to color in this figure legend, the reader is referred to the web version of this article.)

Table 1
Annual mean MODIS-derived AOD, observed downward longwave radiation (DLR), observed air temperature (T_a), observed vapor pressure (e_a) at the Lake Taihu sites.

Variable	site	2011	2012	2013	2014	2015	2016	2017	2018	Trend (yr^{-1})
AOD	BFG	1.10	0.89	1.11	0.86	0.91	0.81	0.78	0.84	−0.038
	DPK	1.21	1.01	1.00	0.70	0.99	1.17	0.71	0.75	−0.046
	DS	1.06	1.07	0.99	1.02	1.04	1.02	0.94	0.95	−0.015
	MLW	0.97	0.99	1.09	0.73	1.06	0.86	0.85	0.88	−0.020
	PTS	1.09	1.01	0.97	0.70	0.91	0.92	1.10	0.82	−0.016
	XLS	1.11	0.89	0.80	0.75	0.93	0.84	0.83	0.91	−0.017
DLR ($W\ m^{-2}$)	BFG	–	362.9	361.5	362.2	365.7	369.5	366.1	368.8	1.22
	DPK	362.0	364.3	365.0	363.9	366.7	370.6	367.7	374.3	1.46
	DS	–	363.1	362.5	352.5	362.0	359.6	353.4	358.5	−0.89
	MLW	357.0	359.1	359.8	359.4	362.6	–	–	–	1.14
	PTS	–	–	–	362.3	365.6	369.7	366.9	369.6	1.60
	XLS	–	–	363.3	363.0	366.7	370.8	367.5	369.8	1.43
T_a (°C)	BFG	–	16.5	17.3	16.9	17.0	17.4	17.7	17.6	0.15
	DPK	–	16.3	17.0	16.6	16.6	17.0	17.6	17.6	0.15
	DS	–	16.5	17.4	17.0	17.1	17.5	17.7	17.6	0.15
	MLW	17.1	16.3	17.0	16.6	16.6	17.4	–	–	0.07
	PTS	–	–	–	17.0	17.0	17.4	17.7	17.6	0.19
	XLS	–	–	17.2	16.8	16.8	17.2	17.5	17.5	0.11
e_a (hPa)	BFG	–	16.3	16.7	15.8	15.8	17.5	17.4	17.8	0.27
	DPK	–	14.8	15.1	15.5	15.9	17.4	16.3	17.9	0.40
	DS	–	14.8	14.5	14.7	14.2	15.1	14.9	15.6	0.13
	MLW	15.3	14.5	14.8	14.4	14.5	16.0	–	–	0.10
	PTS	–	–	–	16.6	16.5	17.2	16.7	16.9	0.07
	XLS	–	–	16.9	16.5	16.5	18.5	18.2	19.0	0.50

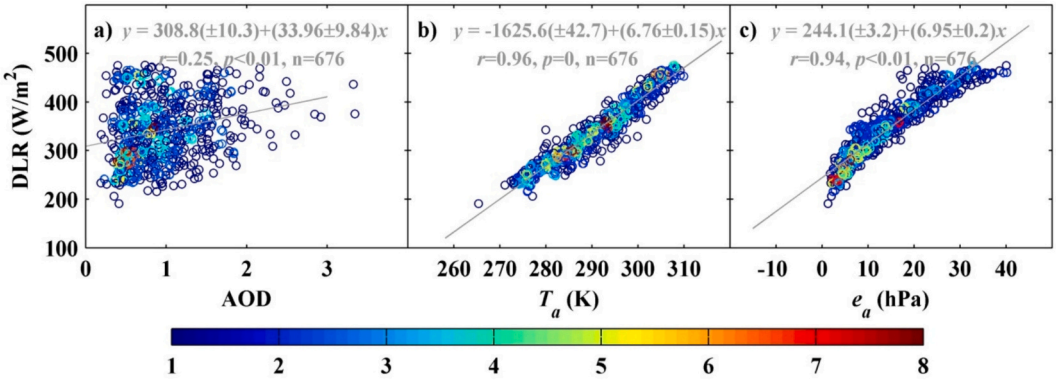

Fig. 3. Scatter plots between observed downward longwave radiation (DLR) and a) MODIS-derived AOD, b) observed air temperature (T_a), and c) observed water vapor pressure (e_a) observed at the six sites. Solid lines represent linear regression with statistics noted. The data density that is categorized from 1 to 8 represents the data number for different colors.

Table 2
Coefficients derived from the three-variable linear regression (eq. 1). Here *b*, *c*, *d* are the sensitivity of observed downward longwave radiation (DLR) to observed air temperature, observed vapor pressure and MODIS-derived AOD, respectively. Parameter bounds for individual sites are 95% confidence intervals. Uncertainties of the mean are ± one standard deviation of spatial replicates.

	b ($W\ m^{-2}\ K^{-1}$)	*c* ($W\ m^{-2}\ hPa^{-1}$)	*d* ($W\ m^{-2}\ AOD^{-1}$)
BFG	4.48 ± 0.41	2.67 ± 0.43	4.72 ± 4.25
DPK	4.07 ± 0.43	2.75 ± 0.41	7.28 ± 3.09
DS	5.44 ± 0.55	2.56 ± 0.62	8.80 ± 6.08
MLW	4.37 ± 0.38	3.07 ± 0.51	3.21 ± 3.09
PTS	4.18 ± 0.59	3.01 ± 0.59	3.43 ± 3.71
XLS	4.27 ± 0.50	2.71 ± 0.47	3.02 ± 5.10
Mean	4.24 ± 0.21	2.98 ± 0.22	4.66 ± 1.99

Similar lower biases were also reported by other researchers (Sun et al., 2019b; Gueymard and Yang, 2020; Che et al., 2022). In comparison, the MERRA-2-derived clear-sky DLR is in much better agreement with the observed DLR, with a regression slope of 1.07 and a mean bias of −39.6 $W\ m^{-2}$ (The MERRA-2 all-sky DLR has a regression slope of 1.07 and a mean bias of −27.6 against the observed DLR). Impressively, T_a and e_a exhibit excellent agreement between MERRA-2 and observations, as indicated by respective slopes of 0.99 for T_a and 1.00 for e_a, along with the small mean biases of 2.3 K and 0.83 hPa.

Table 3
Sensitivity of observed downward longwave radiation to observed air temperature (*b*) and observed vapor pressure (*c*) according to parameterization Eq. (4) and Eq. (5). Calculations were made with observed multi-year mean air temperature and vapor pressure.

	b ($W\ m^{-2}\ K^{-1}$)	*c* ($W\ m^{-2}\ hPa^{-1}$)
BFG	4.34	3.24
DPK	4.33	3.25
DS	4.48	3.49
MLW	4.11	3.80
PTS	4.29	3.14
XLS	4.39	3.00
Mean	4.32	3.33

Table 4 presents the sensitivity results obtained from the MERRA-2 data via two calculation methods. The multivariate linear regression gives a DLR sensitivity of 3.82 (±0.11) $W\ m^{-2}\ K^{-1}$ to T_a and 3.99

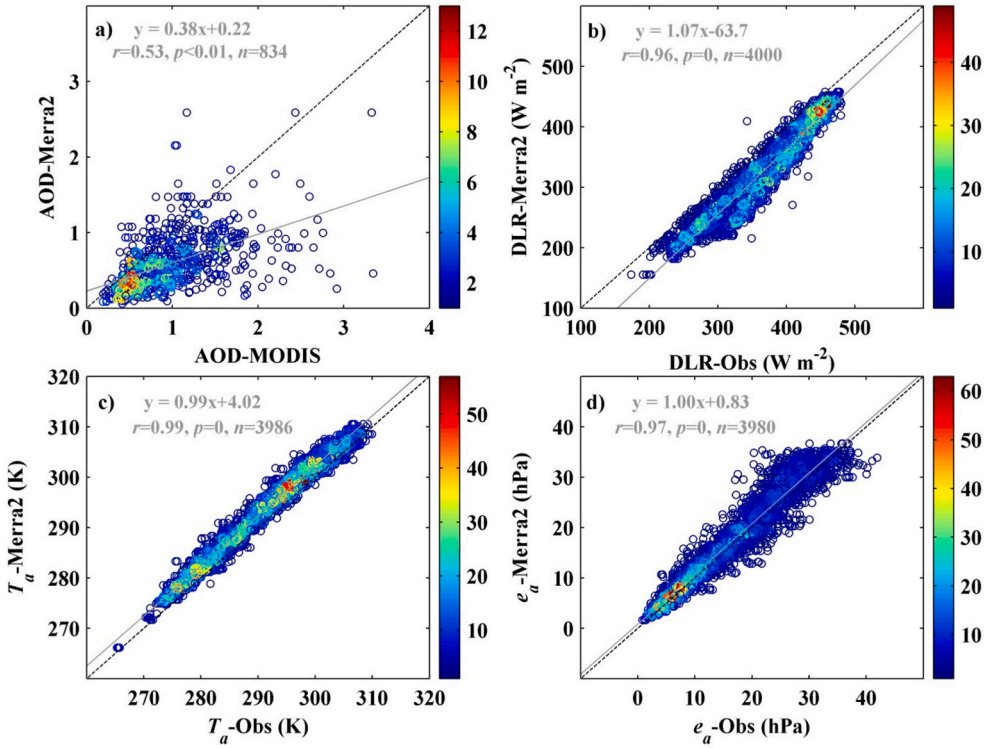

Fig. 4. Comparisons of a) MODIS-retrieved AOD and MERRA-2 AOD, b) observed DLR and MERRA-2 clear-sky DLR, c) observed T_a and MERRA-2 T_a, d) observed e_a and MERRA-2 e_a. Grey solid lines represent linear regression with statistics noted. Dash lines are 1:1. Color indicates data density.

Table 4
Sensitivity results based on MERRA-2 data. Top line: coefficients from three-variable linear regression (Eq. 1); Bottom: Sensitivity to AOD from the difference between DLR with aerosol loading (DLR_{aero}) and DLR without aerosols (DLR_{noaero}) per unit change of AOD. Parameter bounds are 95% confidence intervals.

	b (W m^{-2} K^{-1})	c (W m^{-2} hPa^{-1})	d (W m^{-2} AOD^{-1})
Multivariate regression	3.82 ± 0.11	3.99 ± 0.11	12.00 ± 1.27 (4.56 ± 0.48)*
(DLR_{aero}-DLR_{noaero})/AOD	–	–	4.10 ± 0.25

* The sensitivity in bracket is obtained by using AOD value adjusted with the relationship between MERRA-2 and MODIS AOD (i.e., AOD_{merra2} = 0.38*AOD_{modis} + 0.22).

(±0.11) W m^{-2} hPa^{-1} to e_a, which are in general agreement with the results derived from observations. However, the sensitivity of DLR to AOD (12.0 ± 1.27 W m^{-2} AOD^{-1}) is much larger than that derived from the observational data. The reason is that MERRA-2 AOD is substantially smaller than the MODIS AOD. The MERRA-2 sensitivity is reduced to 4.56 ± 0.48 W m^{-2} AOD^{-1} after the MERRA-2 AOD is adjusted using the linear relationship between MERRA-2 and MODIS AOD shown in Fig. 4a.

Alternatively, the sensitivity of DLR to AOD can be determined through a regression of the DLR difference between the presence and absence of aerosol scenarios against the corresponding AOD difference. Such calculation has been widely used in other studies (e.g., Cao et al., 2016; Panicker et al., 2008). This approach yields a sensitivity of 4.10 (±0.25) W m^{-2} AOD^{-1} (Fig. S2 and Table 4), which agrees well with the observed result (4.66 ± 1.99 W m^{-2} AOD^{-1}).

3.4. SBDART model calculation

Next we aimed to determine whether the DLR sensitivity to AOD obtained from the radiative transfer model is consistent with the results derived from observations. Fig. 5 shows the SBDART-simulated DLR forcing under varying AOD conditions in the Lake Taihu. It is seen that the simulated DLRF has a significant linear relationship with the AOD, and the slope of the fit is 4.69 (±1.23) W m^{-2} AOD^{-1}. Such value is fairly consistent with the sensitivity value obtained by the multivariate linear regression based on the Lake Taihu observations and MERRA-2 reanalysis data.

Fig. 6a further illustrates the simulated DLRF under varying AOD conditions for four distinct aerosol types: rural, urban, oceanic and dust. These simulations utilize the averaged radio sounding vertical profiles during 2011–2018 to represent atmospheric conditions over the Lake Taihu region. The optical parameters of dust aerosols are specified with

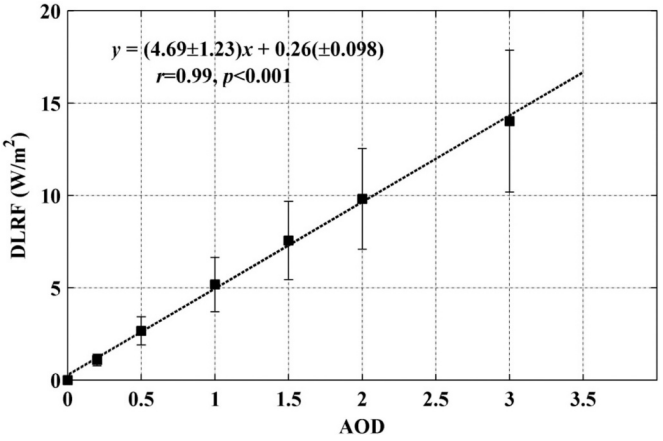

Fig. 5. SBDART-simulated downward longwave radiative forcing (DLRF) as a function of AOD in the Lake Taihu. Uncertainties of the mean are ± one standard deviation of temporal replicates. Lines represent linear regression with statistics noted.

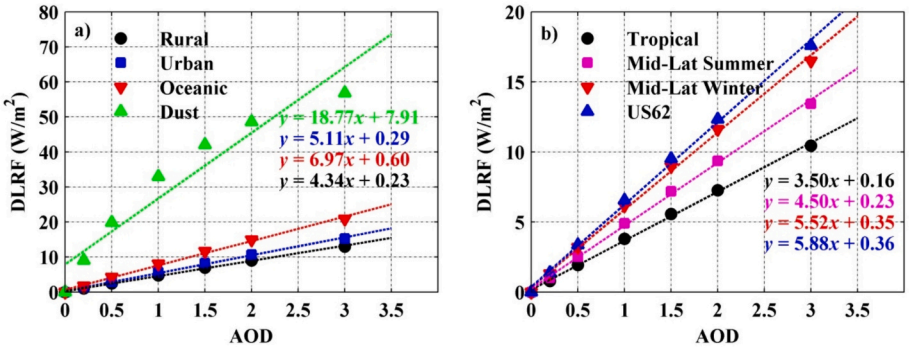

Fig. 6. SBDART-simulated downward longwave radiative forcing (DLRF) as a function of AOD a) for four different aerosol types and b) for four different model atmospheres. Lines represent linear regression with statistics noted.

the output of Optical Properties of Aerosols and Clouds (OPAC) model (Hess et al., 1998), whereas other aerosol types are defined by the SBDART model (see Fig. S3). For the rural aerosol type, the linear regression slope of DLRF against AOD is 4.34 W m^{-2} AOD^{-1}. The slope is slightly higher at 5.11 W m^{-2} AOD^{-1} for the urban aerosol type. Remarkably, dust aerosols exhibit the steepest regression slope (18.77 W m^{-2} AOD^{-1}), followed by oceanic aerosols (6.97 W m^{-2} AOD^{-1}). Our Lake Taihu results fall within the range of sensitivity values obtained from rural and urban aerosols, further demonstrated that rural and urban aerosols are good proxies for the aerosols in the Lake Taihu region (Tao et al., 2020).

Atmosphere conditions also affect the DLR and its sensitivity to AOD. Fig. 6b shows DLRF variations with AOD under four model atmosphere conditions: Tropical, Mid-Latitude Summer, Mid-Latitude Winter, and US62. The regression slope varies from 3.5 W m^{-2} AOD^{-1} for Tropical Atmosphere to 5.88 W m^{-2} AOD^{-1} for US62 Atmosphere. Particularly, in the Tropical Atmosphere, high water vapor longwave forcing occurs, which masks the actual aerosol forcing. The conclusion drawn from these calculations underscores the strengthened sensitivity of DLR to AOD in drier and cooler atmosphere conditions.

4. Discussion

The three estimates of dDLR/dAOD, derived from observational data, reanalysis data and the radiative transfer model, are consistent with each other, but are generally lower than the sensitivity values reported in the literature (e.g., Markowicz et al., 2003; Panicker et al., 2008; Antón et al., 2014; Hansell et al., 2010, 2012; Cao et al., 2016; Maghrabi et al., 2022). Several factors may explain this discrepancy.

Firstly, the sensitivity of DLR to AOD depends on aerosol chemical and physical properties. Distinct aerosol types exhibit varying compositions. Rural aerosols are made up of water soluble and insoluble components (Ramachandran and Kedia, 2012). Urban aerosols are mixtures of the rural aerosols with carbonaceous particles. Oceanic aerosols are composed of sea spray droplets and a continental component similar to the rural aerosols except that most of the very large particles are absent (Shettle and Fenn, 1976). Dust aerosols are composed of mineral particles (Hansell et al., 2010). Urban aerosols, which contain more black carbon, have a lower SSA (Fig. S3) and thus a larger DLR forcing than rural aerosols (Fig. 6a). Hansell et al. (2010) found that variations in dust composition yield large differences in the surface DLR forcing due to the unique absorption features associated with pure minerals in the thermal wavelengths. In addition, aerosol size matters. According to Dufresne et al. (2002) and Hansell et al. (2010), the DLR forcing at the surface strongly increases as the effective radius of dust particle increases due to the enhancement of longwave scattering and absorption. Indeed, as shown in Fig. 6a, the radiative forcing associated with dust aerosol (large particle size) is much larger than that induced by other finer aerosol types (e.g., urban, rural) under the same AOD condition. Moreover, the dust DLR forcing shows non-linearly variation with AOD, thus yielding different sensitivity values at different AOD levels.

Secondly, meteorological condition (e.g., humidity and temperature) can affect the sensitivity of DLR to AOD. Our SBDART model results suggest that dDLR/dAOD is larger under drier and cooler atmosphere conditions than in hotter and more humid environments (Fig. 6b). As depicted in Fig. 2, the temperature and water vapor content at the Lake Taihu is highest in the summer and lowest in the winter. We performed additional three-variable regressions by using MERRA-2 data for the months of July and December. The results show that dDLR/dAOD is 2.86 W m^{-2} AOD^{-1} in July, significantly smaller than the value observed in December, which is 7.04 W m^{-2} AOD^{-1} (In this analysis, the MERRA-2 AOD has been adjusted to remove biases in the regressions). Previous studies support our results that surface DLR forcing decreases with increasing water vapor content (Markowicz et al., 2003; Ramachandran et al., 2006; Panicker et al., 2008). The physical explanation is that the absorption and reemission of DLR by water vapor molecules are more dominant than those of aerosols in warmer and more humid atmospheres.

The third factor is related to clouds. It is important to emphasize that the dDLR/dAOD estimates presented in this study are applicable exclusively under cloud-free conditions. However, clouds can increase DLR due to its high emissivity and high temperature relative to the clear atmosphere. A slightly larger dDLR/dAOD value (6.01 ± 0.75 W m^{-2} AOD^{-1}) is obtained if the MERRA-2 all-sky DLR is used to perform three-variable regression (In this regression analysis, the MERRA-2 AOD has been adjusted to remove biases).

5. Conclusions

In this study, through the application of three-variable linear regression to the observational data, it is found that an increase of one unit AOD resulted in a DLR increase of 4.66 (± 1.99) W m^{-2} and the sensitivity of DLR to temperature and humidity was 4.24 (± 0.21) W m^{-2} K^{-1} and 2.98 (± 0.22) W m^{-2} hPa^{-1}, respectively. The same regression analysis of the MERRA-2 data yields a similar sensitivity to AOD (4.56 ± 0.48 W m^{-2} AOD^{-1}) after the MERRA-2 AOD has been bias-corrected. Furthermore, the sensitivity of DLR to AOD determined as the difference in the MERRA-2 DLR between pollution and aerosol-free scenarios (4.10 ± 0.25 W m^{-2} AOD^{-1}) was in agreement with the values derived from the three-variable linear regression. The SBDART model yields a sensitivity of (4.69 ± 1.23) W m^{-2} AOD^{-1}. These four estimates vary in a narrow range of 4.10 to 4.69 W m^{-2} AOD^{-1}, representing approximately 10% of the grand mean of the estimates (4.51 W m^{-2} AOD^{-1}). These sensitivity values were determined under clear-sky conditions, and it is noteworthy that they are lower than the sensitivity values found in the literature which vary in the range of 4.9 to 62 W m^{-2} AOD^{-1}.

Our findings contribute significantly to enhancing our understanding of the aerosol impact on DLR over the Lake Taihu region in Eastern China. Furthermore, they shed light on the variability of DLR sensitivity to AOD under various background conditions and aerosol types. By elucidating the nuanced relationship between DLR and AOD, this study advances our comprehension of radiative transfer dynamics in a region marked by its significance in the broader global energy budget. The implications of these findings extend to improved accuracy in numerical weather forecasts and further refinement of climate models.

CRediT authorship contribution statement

Cheng Liu: Conceptualization, Methodology, Software, Writing – original draft. **Jianping Huang:** Writing – review & editing, Supervision, Funding acquisition. **Cheng Hu:** Writing – review & editing, Methodology. **Chang Cao:** Writing – review & editing, Methodology. **Kun Yue:** Writing – review & editing, Data curation. **Xiaozhen Fang:** Writing – review & editing. **Renguo Zhu:** Writing – review & editing. **Xuhui Lee:** Writing – review & editing, Supervision, Conceptualization.

Declaration of competing interest

The authors declare that they have no known competing financial interests or personal relationships that could have appeared to influence the work reported in this paper.

Data availability

The Lake Taihu observational data is available online at https://yncenter.sites.yale.edu/data-access and from the Harvard Dataverse (https://doi.org/10.7910/DVN/HEWCWM; Zhang et al., 2020). The MODIS level 2 aerosol products can be downloaded freely via https://ladsweb.modaps.eosdis.nasa.gov/archive/allData/61/MOD04_3K/ and https://ladsweb.modaps.eosdis.nasa.gov/archive/allData/61/MYD04_3K/. The MERRA-2 dataset used for this study is publicly available in: https://disc.gsfc.nasa.gov/datasets?project=MERRA-2.

Acknowledgement

The research was supported jointly by the National Natural Science Foundation of China (42105088) and the Doctoral Research Startup Foundation of East China University of Technology (DHBK2019255). The computing for the SBDART sensitivity experiments were performed at the OU Supercomputing Center for Education and Research (OSCER) at the University of Oklahoma (OU).

Appendix A. Supplementary data

Supplementary data to this article can be found online at https://doi.org/10.1016/j.atmosres.2024.107444.

References

Antón, M., Valenzuela, A., Mateos, D., Alados, I., Foyo-Moreno, I., Olmo, F.J., Alados-Arboledas, L., 2014. Longwave aerosol radiative effects during an extreme desert dust event in southeastern Spain. Atmos. Res. 149, 18–23. https://doi.org/10.1016/j.atmosres.2014.05.022.

Brunt, D., 1932. Notes on radiation in the atmosphere. I. Q. J. R. Meteorol. Soc. 58 (247), 389–420. https://doi.org/10.1002/qj.49705824704.

Brutsaert, W., 1975. On a derivable formula for long-wave radiation from clear skies. Water Resour. Res. 11 (5), 742–744. https://doi.org/10.1029/WR011i005p00742.

Cao, C., Lee, X., Liu, S., Schultz, N., Xiao, W., Zhang, M., Zhao, L., 2016. Urban heat islands in China enhanced by haze pollution. Nat. Commun. 7 (1), 1–7. https://doi.org/10.1038/ncomms12509.

Cao, S., Zhang, S., Gao, C., Yan, Y., Bao, J., Su, L., Liu, M., 2021. A long-term analysis of atmospheric black carbon MERRA-2 concentration over China during 1980–2019. Atmos. Environ. 264, 118662 https://doi.org/10.1016/j.atmosenv.2021.118662.

Che, Y., Yu, B., Parsons, K., Desha, C., Ramezani, M., 2022. Evaluation and comparison of MERRA-2 AOD and DAOD with MODIS DeepBlue and AERONET data in Australia. Atmos. Environ. 277, 119054 https://doi.org/10.1016/j.atmosenv.2022.119054.

Cho, H.K., Kim, J., Jung, Y., Lee, Y.G., Lee, B.Y., 2008. Recent changes in downward longwave radiation at King Sejong Station, Antarctica. J. Clim. 21 (22), 5764–5776. https://doi.org/10.1175/2008JCLI1876.1.

Dufresne, J.L., Gautier, C., Ricchiazzi, P., Fouquart, Y., 2002. Longwave scattering effects of mineral aerosols. J. Atmos. Sci. 59 (12), 1959–1966. https://doi.org/10.1175/1520-0469(2002)059<1959:LSEOMA>2.0.CO;2.

Durre, I., Yin, X., Vose, R.S., Applequist, S., Arnfield, J., 2016. Integrated Global Radiosonde Archive (IGRA), Version 2. NOAA National Centers for Environmental Information. https://doi.org/10.7289/V5X63K0Q.

Filonchyk, M., Yan, H., Zhang, Z., Yang, S., Li, W., Li, Y., 2019. Combined use of satellite and surface observations to study aerosol optical depth in different regions of China. Sci. Rep. 9 (1), 1–15. https://doi.org/10.1038/s41598-019-42466-6.

García, R.D., Barreto, A., Cuevas, E., Gröbner, J., García, O.E., Gómez-Peláez, A., Ramos, R., 2018. Comparison of observed and modeled cloud-free longwave downward radiation (2010–2016) at the high mountain BSRN Izaña station. Geosci. Model Dev. 11 (6), 2139–2152. https://doi.org/10.5194/gmd-11-2139-2018.

Gelaro, R., McCarty, W., Suárez, M.J., Todling, R., Molod, A., Takacs, L., Zhao, B., 2017. The modern-era retrospective analysis for research and applications, version 2 (MERRA-2). J. Clim. 30 (14), 5419–5454. https://doi.org/10.1175/JCLI-D-16-0758.1.

Gueymard, C.A., Yang, D., 2020. Worldwide validation of CAMS and MERRA-2 reanalysis aerosol optical depth products using 15 years of AERONET observations. Atmos. Environ. 225, 117216 https://doi.org/10.1016/j.atmosenv.2019.117216.

Hansell, R.A., Tsay, S.C., Ji, Q., Hsu, N.C., Jeong, M.J., Wang, S.H., Ou, S.C., 2010. An assessment of the surface longwave direct radiative effect of airborne Saharan dust during the NAMMA field campaign. J. Atmos. Sci. 67 (4), 1048–1065. https://doi.org/10.1175/2009JAS3257.1.

Hansell, R.A., Tsay, S.C., Hsu, N.C., Ji, Q., Bell, S.W., Holben, B.N., Chen, H., 2012. An assessment of the surface longwave direct radiative effect of airborne dust in Zhangye, China, during the Asian Monsoon Years field experiment (2008). J. Geophys. Res. Atmos. 117 (D16) https://doi.org/10.1029/2011JD017370.

He, L., Wang, L., Huang, B., Wei, J., Zhou, Z., Zhong, Y., 2020. Anthropogenic and meteorological drivers of 1980–2016 trend in aerosol optical and radiative properties over the Yangtze River Basin. Atmos. Environ. 223, 117188 https://doi.org/10.1016/j.atmosenv.2019.117188.

Hess, M., Koepke, P., Schult, I., 1998. Optical properties of aerosols and clouds: the software package OPAC. Bull. Am. Meteorol. Soc. 79 (5), 831–844. https://doi.org/10.1175/1520-0477(1998)079<0831:OPOAAC>2.0.CO;2.

Huang, X., Ding, A., Wang, Z., Ding, K., Gao, J., Chai, F., Fu, C., 2020. Amplified transboundary transport of haze by aerosol–boundary layer interaction in China. Nat. Geosci. 13 (6), 428–434. https://doi.org/10.1038/s41561-020-0583-4.

Idso, S.B., 1981. A set of equations for full spectrum and 8-to 14-μm and 10.5-to 12.5-μm thermal radiation from cloudless skies. Water Resour. Res. 17 (2), 295–304. https://doi.org/10.1029/WR017i002p00295.

Lee, X., Liu, S., Xiao, W., Wang, W., Gao, Z., Cao, C., Zhang, M., 2014. The Taihu Eddy Flux Network: an observational program on energy, water, and greenhouse gas fluxes of a large freshwater lake. Bull. Am. Meteorol. Soc. 95 (10), 1583–1594. https://doi.org/10.1175/BAMS-D-13-00136.1.

Levy, R., Hsu, C., et al., 2015. MODIS Atmosphere L2 Aerosol Product. NASA MODIS Adaptive Processing System, Goddard Space Flight Center, USA. https://doi.org/10.5067/MODIS/MOD04_L2.061.

Liu, J., Zheng, Y., Li, Z., Flynn, C., Cribb, M., 2012. Seasonal variations of aerosol optical properties, vertical distribution and associated radiative effects in the Yangtze Delta region of China. J. Geophys. Res. Atmos. 117 (D16) https://doi.org/10.1029/2011JD016490.

Liu, C., Fedorovich, E., Huang, J., Hu, X.M., Wang, Y., Lee, X., 2019. Impact of aerosol shortwave radiative heating on entrainment in the atmospheric convective boundary layer: a large-eddy simulation study. J. Atmos. Sci. 76 (3), 785–799. https://doi.org/10.1175/JAS-D-18-0107.1.

Liu, C., Huang, J., Tao, X., Deng, L., Fang, X., Liu, Y., Xiao, H.Y., 2021. An observational study of the boundary-layer entrainment and impact of aerosol radiative effect under aerosol-polluted conditions. Atmos. Res. 250, 105348 https://doi.org/10.1016/j.atmosres.2020.105348.

Maghrabi, A.H., Almutayri, M.M., Aldosary, A.F., Allehyani, B.I., Aldakhil, A.A., Aljarba, G.A., Altilasi, M.I., 2019. The influence of atmospheric water content, temperature, and aerosol optical depth on downward longwave radiation in arid conditions. Theor. Appl. Climatol. 138 (3), 1375–1394. https://doi.org/10.1007/s00704-019-02903-y.

Maghrabi, A., Alharbi, B., Alharbi, H., Aldosari, A., 2022. Correlation analyses between downward longwave radiation particulate matters, aerosol optical depth, and metrological variables under non-dusty and cloudless conditions. Theor. Appl. Climatol. 148, 1577–1586. https://doi.org/10.1007/s00704-022-04004-9.

Markowicz, K.M., Flatau, P.J., Vogelmann, A.M., Quinn, P.K., Welton, E.J., 2003. Clear-sky infrared aerosol radiative forcing at the surface and the top of the atmosphere. Q. J. R. Meteorol. Soc. 129 (594), 2927–2947. https://doi.org/10.1256/qj.02.224.

Panicker, A.S., Pandithurai, G., Safai, P.D., Kewat, S., 2008. Observations of enhanced aerosol longwave radiative forcing over an urban environment. Geophys. Res. Lett. 35 (4), L04817. https://doi.org/10.1029/2007GL032879.

Prata, A.J., 1996. A new long-wave formula for estimating downward clear-sky radiation at the surface. Q. J. R. Meteorol. Soc. 122 (533), 1127–1151. https://doi.org/10.1002/qj.49712253306.

Ramachandran, S., Kedia, S., 2012. Radiative effects of aerosols over Indo-Gangetic plain: environmental (urban vs. rural) and seasonal variations. Environ. Sci. Pollut. Res. 19, 2159–2171. https://doi.org/10.1007/s11356-011-0715-x.

Ramachandran, S., Rengarajan, R., Jayaraman, A., Sarin, M.M., Das, S.K., 2006. Aerosol radiative forcing during clear, hazy, and foggy conditions over a continental polluted location in north India. J. Geophys. Res. Atmos. 111 (D20) https://doi.org/10.1029/2006JD007142.

Remer, L.A., Mattoo, S., Levy, R.C., Munchak, L.A., 2013. MODIS 3 km aerosol product: algorithm and global perspective. Atmos. Meas. Tech. 6 (7), 1829–1844. https://doi.org/10.5194/amt-6-1829-2013.

Ricchiazzi, P., Yang, S., Gautier, C., Sowle, D., 1998. SBDART: a research and teaching software tool for plane-parallel radiative transfer in the Earth's atmosphere. Bull. Am. Meteorol. Soc. 79 (10), 2101–2114. https://doi.org/10.1175/1520-0477(1998)079<2101:SARATS>2.0.CO;2.

Shettle, E.P., Fenn, R.W., 1976. Models of the atmospheric aerosols and their optical properties. AGARD Conference Proceedings, no. 183 AGARD-CP–183.

Shu, L., Xie, M., Gao, D., Wang, T., Fang, D., Liu, Q., Peng, L., 2017. Regional severe particle pollution and its association with synoptic weather patterns in the Yangtze River Delta region, China. Atmos. Chem. Phys. 17 (21), 12871–12891. https://doi.org/10.5194/acp-17-12871-2017.

Sun, K., Liu, H., Wang, X., Peng, Z., Xiong, Z., 2017. The aerosol radiative effect on a severe haze episode in the Yangtze River Delta. J. Meteorol. Res. 31 (5), 865–873. https://doi.org/10.1007/s13351-017-7007-4.

Sun, T., Che, H., Qi, B., Wang, Y., Dong, Y., Xia, X., Zhang, X., 2019a. Characterization of vertical distribution and radiative forcing of ambient aerosol over the Yangtze River Delta during 2013–2015. Sci. Total Environ. 650, 1846–1857. https://doi.org/10.1016/j.scitotenv.2018.09.262.

Sun, E., Che, H., Xu, X., Wang, Z., Lu, C., Gui, K., Shi, G., 2019b. Variation in MERRA-2 aerosol optical depth over the Yangtze River Delta from 1980 to 2016. Theor. Appl. Climatol. 136 (1), 363–375. https://doi.org/10.1007/s00704-018-2490-9.

Tao, M., Wang, L., Chen, L., Wang, Z., Tao, J., 2020. Reversal of aerosol properties in eastern China with rapid decline of anthropogenic emissions. Remote Sens. 12 (3), 523. https://doi.org/10.3390/rs12030523.

Viúdez-Mora, A., Calbó, J., González, J.A., Jiménez, M.A., 2009. Modeling atmospheric longwave radiation at the surface under cloudless skies. J. Geophys. Res. Atmos. 114 (D18) https://doi.org/10.1029/2009JD011885.

Vogelmann, A.M., Flatau, P.J., Szczodrak, M., Markowicz, K.M., Minnett, P.J., 2003. Observations of large aerosol infrared forcing at the surface. Geophys. Res. Lett. 30 (12) https://doi.org/10.1029/2002GL016829.

Wacker, S., Gröbner, J., Hocke, K., Kämpfer, N., Vuilleumier, L., 2011. Trend analysis of surface cloud-free downwelling long-wave radiation from four Swiss sites. J. Geophys. Res. Atmos. 116 (D10) https://doi.org/10.1029/2010JD015343.

Wang, K., Liang, S., 2009. Global atmospheric downward longwave radiation over land surface under all-sky conditions from 1973 to 2008. J. Geophys. Res. Atmos. 114 (D19) https://doi.org/10.1029/2009JD011800.

Wang, C., Tang, B.H., Wu, H., Tang, R., Li, Z.L., 2017. Estimation of downwelling surface longwave radiation under heavy dust aerosol sky. Remote Sens. 9 (3), 207. https://doi.org/10.3390/rs9030207.

Xiao, W., Zhang, Z., Wang, W., Zhang, M., Liu, Q., Hu, Y., Lee, X., 2020. Radiation controls the interannual variability of evaporation of a subtropical lake. J. Geophys. Res. Atmos. 125 (8) https://doi.org/10.1029/2019JD031264 e2019JD031264.

Xu, X., Liu, C., Wang, J., Yin, Y., Zhu, X., 2022. Long-term multidataset direct aerosol radiative forcing and its efficiencies: intercomparisons and uncertainties. Atmos. Res. 267, 105964 https://doi.org/10.1016/j.atmosres.2021.105964.

Yu, L., Zhang, M., Wang, L., Qin, W., Li, J., 2019. Aerosol radiative effects from observations and modelling over the Yangtze River Basin, China from 2001 to 2015. Int. J. Climatol. 39 (8), 3476–3491. https://doi.org/10.1002/joc.6033.

Zhang, Q., Geng, G., 2019. Impact of clean air action on $PM_{2.5}$ pollution in China. Sci. China Earth Sci. 62 (12), 1845–1846. https://doi.org/10.1007/s11430-019-9531-4.

Zhang, Z., Zhang, M., Cao, C., Wang, W., Xiao, W., Xie, C., Lee, X., 2020. A dataset of microclimate and radiation and energy fluxes from the Lake Taihu eddy flux network. Earth Syst. Sci. Data 12 (4), 2635–2645. https://doi.org/10.5194/essd-12-2635-2020.

Zhuang, B., Wang, T., Liu, J., Che, H., Han, Y., Fu, Y., Sun, J., 2018. The optical properties, physical properties and direct radiative forcing of urban columnar aerosols in the Yangtze River Delta, China. Atmos. Chem. Phys. 18 (2), 1419–1436. https://doi.org/10.5194/acp-18-1419-2018.